Research Article

Daming Luo, Fan Li, and Guohua Xing*

Corrosion resistance of 6061-T6 aluminium alloy and its feasibility of near-surface reinforcements in concrete structure

https://doi.org/10.1515/rams-2022-0048
received January 07, 2022; accepted July 09, 2022

Abstract: The durability of concrete structures is often reduced owing to the corrosion of reinforcement in an aggressive environment. Ordinary reinforcement methods, such as wrapping section steel or steel plate, are also vulnerable to corrosion. Using 6061-T6 aluminium alloy as near-surface reinforcement of the concrete structure is a feasible method. In this study, the corrosion resistance of 6061-T6 aluminium alloy bars was studied by simulating the coastal environment, atmospheric environment, and concrete internal environment with chloride solution, simulated acid rain solution, and saturated $Ca(OH)_2$ solution. The corrosion rate of the 6061-T6 aluminium alloy in the above environments was tested using a weight loss method, and its corrosion resistance was evaluated using the metal corrosion resistance classification standard. Based on the electrochemical reaction mechanism, the polarisation properties and AC impedance spectra of steel and 6061-T6 aluminium alloy were compared, and the corrosion resistance mechanisms of steel and the 6061-T6 aluminium alloy in the above corrosive environments were obtained. The results show that the 6061-T6 aluminium alloy has better corrosion resistance than steel bars in chloride and atmospheric environments, with corrosion currents of 0.012 and 0.037 $\mu A \cdot cm^{-2}$, and 8-day corrosion rates of 0.051 and 0.031 $mm \cdot a^{-1}$, respectively. However, owing to the activity of the aluminium alloy, its corrosion resistance in an alkaline environment inside concrete is poor; the corrosion current is 0.22 $\mu A \cdot cm^{-2}$ and the 8-day corrosion rate is 16.166 $mm \cdot a^{-1}$. The research results can provide a reference for applying aluminium alloy bars as external prestressed concrete bars and near-surface steel bars.

Keywords: 6061-T6 aluminium alloy, chloride, acid rain, alkali, concrete structure

1 Introduction

Steel corrosion will lead to a reduction in the stiffness, ductility, bond behaviour, and deformation performance of reinforced concrete structures [1,2], which seriously weakens the mechanical performance of components and has become the main cause of insufficient durability and premature failure of reinforced concrete buildings. According to statistics, the loss caused by corrosion is greater than that by any other natural disaster [3]. Corrosion, which damages engineering equipment and structures, may lead to catastrophic accidents. In China, for example, the annual loss caused by corrosion is approximately 3–5% of the Chinese gross domestic product [4]. To prevent steel corrosion, a coating or rust inhibitor [5] is usually applied on the surface of the steel. However, it cannot change the properties of steel, which is prone to oxidation. Research and development of new materials to replace steel in civil engineering structures can fundamentally solve the problem of steel corrosion.

More and more existing concrete structures need to be reinforced to meet the durability requirements. At present, the reinforcement methods for concrete members mainly include increasing member section, replacing concrete, wrapping section steel or steel plate, pasting fiber-reinforced materials, etc. Some scholars have adhered fiber-reinforced polymer (FRP) plates to the surface of reinforced concrete beams to improve their bending performance [6,7], or embedded carbon fiber-reinforced polymer in the near-surface of reinforced concrete beams to enhance

* **Corresponding author: Guohua Xing,** School of Civil Engineering, Chang'an University, Xi'an 710061, China,
e-mail: ghxing@chd.edu.cn
Daming Luo: State Key Laboratory of Green Building in Western China, Xi'an University of Architecture and Technology, Xi'an 710055, China; School of Civil Engineering, Xi'an University of Architecture and Technology, Xi'an 710055, China,
e-mail: dmluo@xauat.edu.cn
Fan Li: School of Civil Engineering, Xi'an University of Architecture and Technology, Xi'an 710055, China

their flexural bearing capacity [8,9], fatigue properties [10], and shear capacity [11,12]. Ordinary reinforcement methods, such as external steel plates, are vulnerable to corrosion, and the reinforcement effect is not ideal. Aluminum alloy materials have superior performance compared with ordinary steel bars and have great potential to be used for structural reinforcement material [13,14].

The mineral reserves of aluminium account for approximately one-tenth of the earth's crust. Compared with steel, aluminium alloys have the advantages of high specific strength, light weight, and good corrosion resistance, which is why they are widely used in aerospace [15], machinery, electronics, light industrial building materials, and other fields [16]. Researchers have carried out numerous studies on the mechanical properties of aluminium alloys and have issued specifications and manuals on the structural design of those alloys [17]. These studies mainly focused on the constitutive relations, physical and mechanical properties [18], local stability, and component connection of aluminium alloys. At the same time, a series of studies [19] have been carried out that mainly focused on pitting corrosion, intergranular corrosion, exfoliation corrosion, and stress corrosion cracking of specific aluminium alloy materials, such as AA6063 [20], AA2024 [21,22], AA2090 [23], AA7075 [22], AA7150 [24], and Al/SiCp composites [25] in acid or salt solutions. Additionally, the relationships among the elemental composition, microstructure, processing, and electrochemical corrosion behaviour of aluminium alloys were studied [26,27]. However, with the increasing demand for aluminium alloys in the construction industry, there is insufficient research on the application of aluminium alloys in concrete structures. The 6061-T6 aluminium alloy is a high-quality aluminium alloy product [28] produced during heat treatment and pre-stretching processes. It has excellent processing performance, good welding and electroplating characteristics, good corrosion resistance, high toughness, and no deformation after processing. It is widely used in the large-space grid systems of military and civil buildings [28,29]. However, it is rarely used as a reinforcement in concrete structures. As an active metal, aluminium is easily oxidised in the atmosphere, forming a dense and stiff oxide film (Al_2O_3) with a thickness of approximately 5–10 nm [30]. The corrosion resistance of aluminium alloy largely depends on the integrity and self-repairing ability of the oxide film. The corrosion of the aluminium alloy is the result of its surface oxidation film being destroyed. Aluminium can react with alkali, which is not conducive to the aluminium alloy bar as the stressed bar in concrete. As a result, aluminium alloy bars show great promise for use as external prestressed bars or near-surface reinforcements of concrete structures [31].

In the common service environments of concrete structures, chloride ions and acid media, such as sulfur dioxide, are the main factors leading to the corrosion of aluminium alloys. Sodium chloride is the main solid deposit on the surfaces of metals in the near marine atmospheric environment. It has strong hygroscopicity and can dissolve in a thin liquid film on the surface of aluminium alloys to form a strong corrosive dielectric, accelerating the corrosion of aluminium alloys. As one of the main air pollutants, sulfur dioxide dissolved in water will acidify the thin liquid film on the aluminium alloy surface (forming sulfite or sulfate) and accelerate its corrosion. Calcium hydroxide, the product of cement hydration, dissolves in the pore solution of concrete, which makes concrete alkaline and may corrode the aluminium alloy. Although the 6061-T6 aluminium alloy has good corrosion resistance, its performance in the aforementioned environment needs to be studied experimentally.

In this study, chloride, acid rain, and saturated calcium hydroxide solutions were used to simulate the marine environment, atmospheric environment, and internal environment of concrete, respectively. The corrosion resistance of the 6061-T6 aluminium alloy in the above environments was determined by analysing the corrosion rate, polarisation characteristics, impedance spectroscopy, and metal surface. The feasibility of using aluminium alloy bars as external prestressing tendons and near-surface reinforcing bars in concrete structures will be studied.

2 Materials and methods

2.1 Materials

Analytical reagents and distilled water were used in this study. The pH of the simulated acid rain solution was 4.8, and its composition is given in Table 1. A sodium chloride solution with a mass fraction of 3.5% and a saturated Ca$(OH)_2$ solution were used as the chlorine solution and alkaline solution, respectively.

An HPB300 steel bar and a 6061-T6 aluminium alloy were selected for this test. The chemical compositions of these materials are listed in Tables 2 and 3, respectively. Before the test, the samples were gradually ground smooth with 200#, 400#, 600#, 1000#, and 1200# sandpaper, and then the surfaces of the samples were treated with distilled water. After drying and prior to corrosion testing, the samples were weighed. The prepared samples are shown in Figure 1.

Table 1: Composition of simulated acid rain ($mg \cdot L^{-1}$)

Chemical composition	SO_4^{2-}	NO_3^-	NH_4^+	Ca^{2+}	Mg^{2+}	Cl^-	K^+	Na^+	F^-
Content ($mg \cdot L^{-1}$)	21.940	4.850	3.100	5.670	0.350	1.680	1.030	0.540	0.480

Table 2: Chemical composition of 6061-T6 aluminium alloy (mass fraction, %)

Chemical composition	Mg	Si	Cu	Cr	Fe	Mn	Zn	Ti	Al
Content (%)	0.8–1.2	0.4–0.8	0.13–0.4	0.05–0.35	≤0.7	≤0.15	≤0.25	≤0.15	Bal.

In this test, there were 10 groups with 3 specimens in each group, and the corrosion resistance of 6061-T6 aluminium alloy and HPB300 steel bar immersed in the corrosion solutions for 3 days and 8 days were studied. Considering that the steel bar in the saturated $Ca(OH)_2$ solution at room temperature is in a passive state and no corrosion occurs, the corrosion test of the steel bar in saturated $Ca(OH)_2$ solution was not conducted. The experimental groups are presented in Table 4.

2.2 Experimental methods

2.2.1 Corrosion test

The container used in the corrosion test had a capacity of 50 L. After each solution was prepared, three specimens were placed at a certain distance apart. Glass rods were used to support the test pieces to avoid contact between the test pieces and the bottom of the box, as shown in Figure 2. The experiments were conducted at room temperature.

2.2.2 Corrosion rate test

After a set time elapsed for the corrosion process to occur, the corrosion products of the steel bars in the chloride solution and simulated acid rain solution were removed with flowing water, and the corroded aluminium alloy in the saturated $Ca(OH)_2$ solution was soaked in 10% nitric acid at room temperature for half an hour and then removed.

The weight loss method was used to calculate the corrosion rate ($mm \cdot a^{-1}$) of the sample in the corrosive medium, and the calculation formula is as follows [32]:

$$V = \frac{87{,}600 \times \Delta W}{d \times S \times t}, \tag{1}$$

Table 3: Chemical composition of HPB300 steel bar (mass fraction, %)

Chemical composition	C	Si	Mn	Cr	Cu	P	S	Fe
Content (%)	0.27–0.34	0.9–1.2	0.8–1.1	0.8–1.1	≤0.20	≤0.025	≤0.025	Bal.

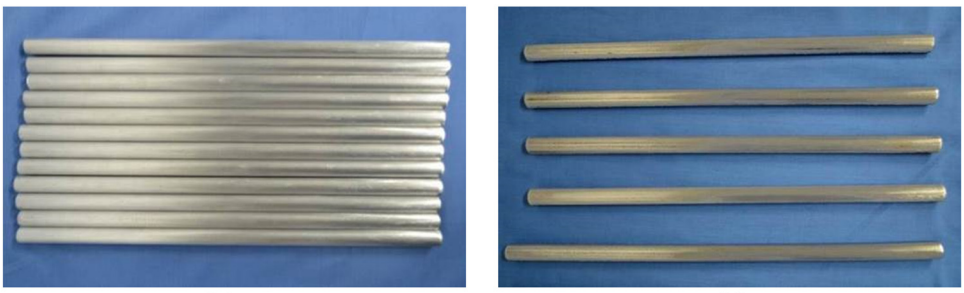

(a) (b)

Figure 1: Specimens used in this study: (a) 6061-T6 aluminium alloy and (b) HPB300 steel bar.

Table 4: Experimental groups

Number	Reinforcement type	Diameter (mm)	Solution	Soaking time (h)
1#	Aluminium alloy	14	Simulated acid rain	72
2#	Aluminium alloy	14	Simulated acid rain	192
3#	Aluminium alloy	14	Chloride solution	72
4#	Aluminium alloy	14	Chloride solution	192
5#	Aluminium alloy	14	Saturated $Ca(OH)_2$ solution	72
6#	Aluminium alloy	14	Saturated $Ca(OH)_2$ solution	192
7#	Steel bar	16	Simulated acid rain	72
8#	Steel bar	16	Simulated acid rain	192
9#	Steel bar	14	Chloride solution	72
10#	Steel bar	14	Chloride solution	192

where V is the corrosion rate ($mm \cdot a^{-1}$), ΔW is the weight loss of the sample (g), d is the density of the sample ($g \cdot cm^{-3}$), S is the surface area of the specimen in contact with the solution (cm^2), and t is the corrosion time (h).

2.2.3 Electrochemical properties

In the electrochemical test, a three-electrode system was employed, in which the working electrode was the HPB300 steel bar or 6061-T6 aluminium alloy and the auxiliary electrode was a platinum electrode. The reference electrode was a saturated calomel electrode when the electrolyte was a chloride solution or simulated acid rain solution. A mercury oxide electrode was used as the reference electrode when the electrolyte was a saturated $Ca(OH)_2$ solution. To ensure the repeatability of the test results, at least three samples were used in the electrochemical test. A Princeton VersaSTAT 3 electrochemical workstation, whose schematic diagram shown in Figure 3, was used in this test.

The working electrode sample had a length of 1 cm and a working area of 1.539 cm^2. Before the experiment, the working surface of the sample was polished and degreased using an acetone solution. After that, it was washed with deionised water and then degreased in an alcohol solution for approximately 5 min. Finally, it was cleaned with deionised water and dried. The specimen was connected to the wire through a small slot, then the non-working part was sealed with epoxy, and only the working face was exposed, as shown in Figure 4.

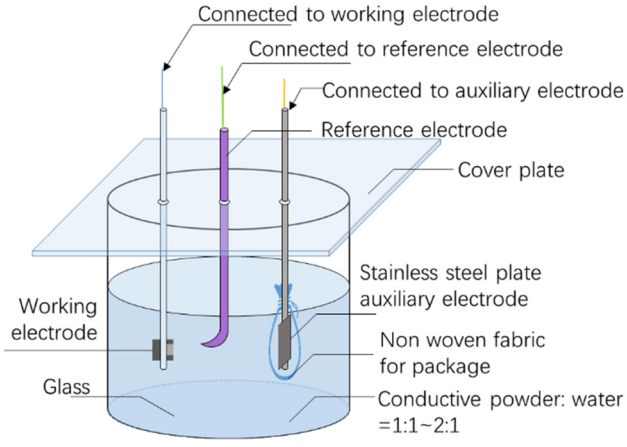

Figure 3: Schematic diagram of a three-electrode system test device.

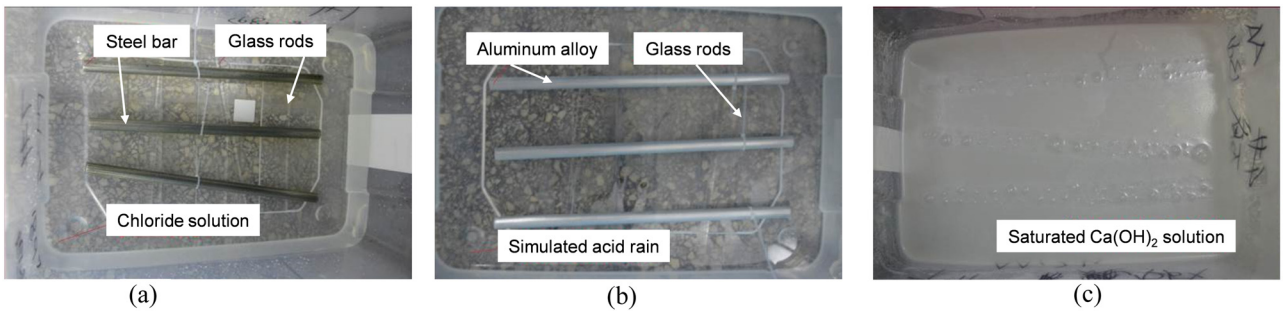

(a) (b) (c)

Figure 2: Corrosion test in different simulated environments: (a) chloride solution, (b) simulated acid rain, and (c) saturated $Ca(OH)_2$ solution.

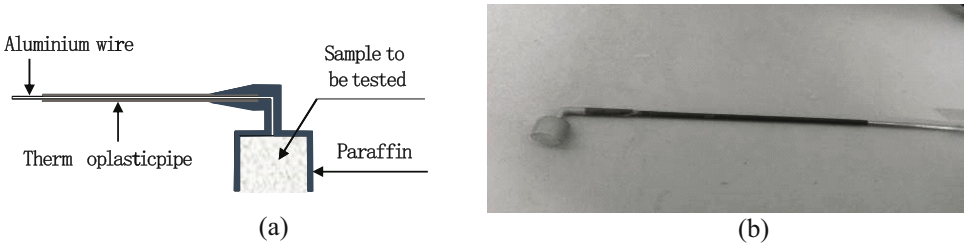

Figure 4: Working electrode and its structure diagram: (a) electrode structure and (b) working electrode.

Electrochemical tests were carried out at room temperature. The scanning potential of the aluminium alloy in saturated $Ca(OH)_2$ was −2.5 to −0.5 V, and the scanning potential of other specimens was −1.5 to −0.3 V. The potential scanning rate was 2 mV·s^{-1}. Electrochemical impedance spectroscopy (EIS) was performed at the open-circuit potential, and the test device was the same as the polarisation curve. A sine-wave AC voltage with an amplitude of 5 mV was applied as the excitation signal. The scanning frequency range was 0.05–2,000 Hz. Before the test, the samples were placed in the test medium for 25 min, and the AC impedance spectrum of the aluminium alloy sample was measured after the potential was stabilised.

2.2.4 Surface analysis experiment

After being immersed in corrosive solutions for a set time, the samples were removed and dehydrated with ethanol at concentrations of 50, 70, 90, and 100% for 15 min and then vacuum dried. The corroded surfaces of 6061-T6 aluminium alloys were investigated using a scanning electron microscopy instrument equipped with an energy-dispersive spectroscopy probe.

3 Results

3.1 Surface state of the specimens

After 72 h of immersion, 1#, 3#, 5#, 7#, and 9# specimens were removed from the solution. As shown in Figure 5, 1# aluminium alloy showed no obvious change, while 3# aluminium alloy had a surface that was both yellow and dark, but there was no corrosion material attached. The 5# aluminium alloy had a layer of black corrosion products that were easy to clean. Both 7# and 9# (steel bars) were coated with yellow corrosion products.

After immersion for 192 h, 2#, 4#, and 6# aluminium alloys and 8# and 10# steel bars were removed from the solution (Figure 6). It can be seen from the figure that there was no obvious corrosion of the aluminium alloy in the simulated acid rain solution and chloride solution, and there was no corrosion product on the surface. However, the corrosion of the aluminium alloy in the saturated $Ca(OH)_2$ solution was considerable, with a layer of black corrosion products on the surface. The steel bar was significantly corroded in the chloride solution and simulated acid rain solution, with a layer of yellow rust

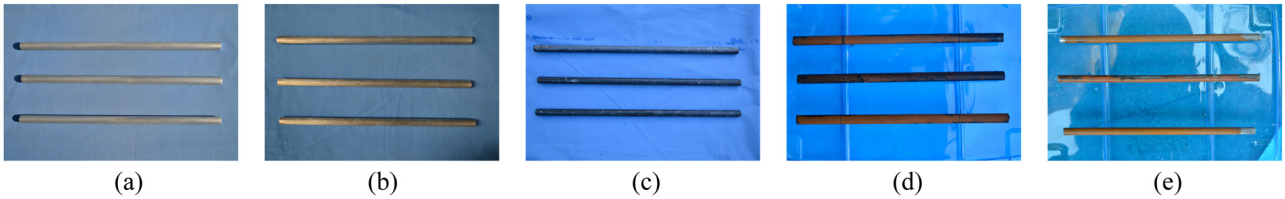

Figure 5: Surface state of the specimens after immersion for 72 h: (a) 1#, (b) 3#, (c) 5#, (d) 7#, and (e) 9#.

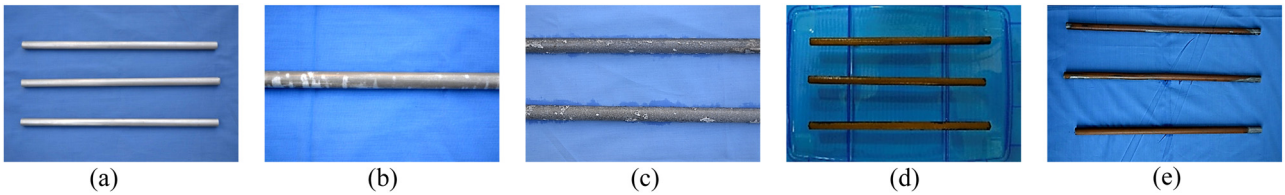

Figure 6: Surface state of the specimens after immersion for 192 h: (a) 2#, (b) 4#, (c) 6#, (d) 8#, and (e) 10#.

Table 5: Corrosion rate of specimens

Number	Reinforcement	Solution	Mass loss rate (%)	Average corrosion rate ($mm \cdot a^{-1}$)
1#	Aluminium alloy	Simulated acid rain	0.002	0.078
2#	Aluminium alloy	Simulated acid rain	0.004	0.058
3#	Aluminium alloy	Chloride solution	0.002	0.078
4#	Aluminium alloy	Chloride solution	0.004	0.059
5#	Aluminium alloy	Saturated $Ca(OH)_2$ solution	0.620	22.572
6#	Aluminium alloy	Saturated $Ca(OH)_2$ solution	1.138	15.553
7#	Steel bar	Simulated acid rain	0.035	1.405
8#	Steel bar	Simulated acid rain	0.090	1.336
9#	Steel bar	Chloride solution	0.027	0.960
10#	Steel bar	Chloride solution	0.061	0.818

on the surface. From this perspective, the application of the aluminium alloy in marine or atmospheric environments has its advantages, but it may have limitations as a stressed bar in direct contact with concrete.

3.2 Calculation of the corrosion rate

After the test, the specimens were removed from the solution, cleaned, and weighed. The corrosion rates of the test specimens were calculated using formula (1). The results are presented in Table 5.

According to *Corrosion of Metals and Alloys* [33], the corrosion resistance of the specimens is classified and graded based on the corrosion rate measured by depth, as shown in Table 6.

It can be seen from the corrosion types of materials and the corrosion rate comparison (Figure 7) that the aluminium alloy has good corrosion resistance in chloride and simulated acid rain solution, while the corrosion resistance of steel bar in the above solutions is worse than that of the aluminium alloy. However, the corrosion resistance of aluminium alloys in saturated $Ca(OH)_2$ solutions is poor.

3.3 Electrochemical performances of the metal materials

3.3.1 Electrochemical performances after chloride corrosion

3.3.1.1 Polarisation behaviour

The polarisation curves of the aluminium alloy and steel bar in the chloride solution are shown in Figure 8. As can be seen from the figure, both the steel bar and the aluminium alloy were controlled by the activation process without obvious "passivation" characteristics. The polarization curve shows that the corrosion voltage of the aluminium alloy and the steel bar were −0.95 and −0.99 V, and the corrosion current values were 0.012 $\mu A \cdot cm^{-2}$ and 0.078 $\mu A \cdot cm^{-2}$, respectively. The self-corrosion potential difference between the aluminium alloy and steel bar is not large, but the self-corrosion current of the aluminium alloy cross-section is smaller than that of the steel bar. The polarisation curve of steel increases sharply when the current density is approximately 0.00004 $A \cdot cm^{-2}$, while that of the aluminium alloy increases sharply when the current density is 0.05 $A \cdot cm^{-2}$. This may be because that chloride ions promote the electrochemical corrosion process in the depolarization of the steel bar anode. When chloride ions invade the surface of the steel bar and damage the passive film, a potential difference between the exposed iron matrix and the passive film is generated, forming a galvanic cell and accelerating the development of pitting corrosion. The chloride ions combine with the anode product Fe^{2+} to form $FeCl_2$ and $Fe(OH)_2$ in water [34]. Free chloride ions can react with Fe^{2+} repeatedly, as chloride ions play a "transport role" without being consumed. However, because of the polarisation of aluminium, $Al(OH)_3$ can easily form and attach to the surface of the aluminium alloy, which effectively hinders Cl^- from entering the electrode matrix to participate in the activation reaction and slows down the activation rate [35]. Therefore, the steel bar in the chlorine solution is more active and more sensitive to Cl^-, and its corrosion rate is higher than that of the aluminium alloy. That is, the aluminium alloy in the chlorine solution is more corrosion-resistant than the steel bar, which is consistent with the conclusion reached in Section 3.2.

3.3.1.2 AC impedance spectroscopy

To verify the polarisation results, the electrochemical impedance spectra of the aluminium alloy and steel bar in the chloride solution were obtained. The variation in

Table 6: Corrosion resistance evaluation of metal materials

Reinforcement	Aluminium alloy			Steel bar		
Corrosive solution	Simulate acid rain solution	Chloride solution	Saturated $Ca(OH)_2$ solution	Simulate acid rain solution	Chloride solution
3 days corrosion rate, $mm \cdot a^{-1}$	0.078	0.078	22.572	1.405	0.960
8 days corrosion rate, $mm \cdot a^{-1}$	0.058	0.059	15.553	1.336	0.818
Corrosion grade	Level 5	Level 5	Level 10	Level 8	Level 7
Corrosion-resistant category	Corrosion-resistant material	Corrosion-resistant material	Non-corrosion-resistant material	Low corrosion-resistant material	Under-corrosion-resistant material

complex impedance with frequency is represented by the Nyquist diagram. According to the principle of AC impedance [36], the diameter of the curve in the Nyquist diagram reflects the impedance value. The larger the semicircle diameter, the better the corrosion resistance. Figure 9 shows the EIS results for the aluminium alloy and steel bar immersed in a 3.5% sodium chloride solution at the open-circuit potential. It can be seen from the figure that the impedance curve diameter of the aluminium alloy is much larger than that of the steel bar, indicating that the corrosion resistance of the aluminium alloy in the chlorine solution is better than that of the steel bar, which is consistent with the conclusion drawn above.

3.3.2 Electrochemical characteristics under acid rain corrosion

3.3.2.1 Polarisation behaviour

Figure 10 shows the polarisation curves of the steel bar and aluminium alloy in the simulated acid rain solution. It can be seen from the figure that the corrosion voltage of the aluminium alloy was –1.02 V, and the corrosion current was 0.037 $\mu A \cdot cm^{-2}$. The corrosion voltage of the steel bar was –1.12 V, and the corrosion current was 0.082 $\mu A \cdot cm^{-2}$. The corrosion current of the aluminium alloy is lower than that of the steel bar, indicating that the anti-corrosion performance of the aluminium alloy in the simulated acid rain solution is better than that of the steel bar. This is because the thickness and integrity of the oxide film on the surface of the aluminium alloy remained unchanged in the simulated acid rain solution of pH 4.8. However, the passive film on the surface of the steel bar was destroyed under simulated acid rain conditions, which caused the steel bar to change to the active state, causing electrochemical corrosion. The metal in the corrosion pits of the steel bar and the passive film form a "membrane-pitting battery." $Fe(OH)_3$ generated from the battery is deposited in the pit orifice, which causes oxygen in the pitting to decrease, thus forming an oxygen concentration difference battery [37]. The ionisation in the hole is accelerated, and the ion migration outside the hole forms a complex with Fe^{2+}; thus, pitting corrosion develops continuously. It can be seen from the corrosion mechanism that the corrosion resistance of the aluminium alloy is far greater than that of the steel bar in the simulated acid rain solution.

3.3.2.2 AC impedance spectroscopy

Figure 11 shows the AC impedance spectra of the aluminium alloy and steel bar in the simulated acid rain

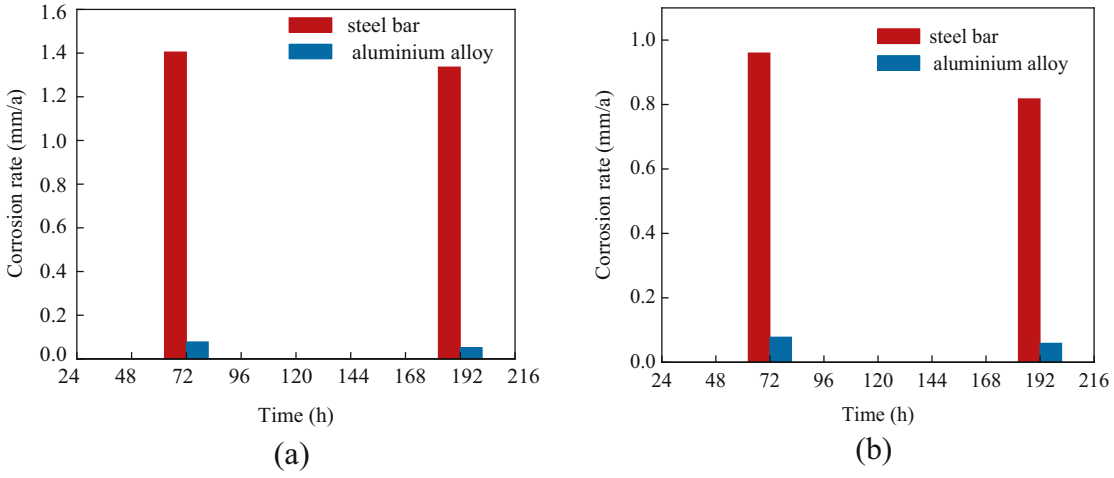

Figure 7: Comparison of corrosion rate between aluminum alloy and steel bar: (a) simulated acid rain and (b) chloride solution.

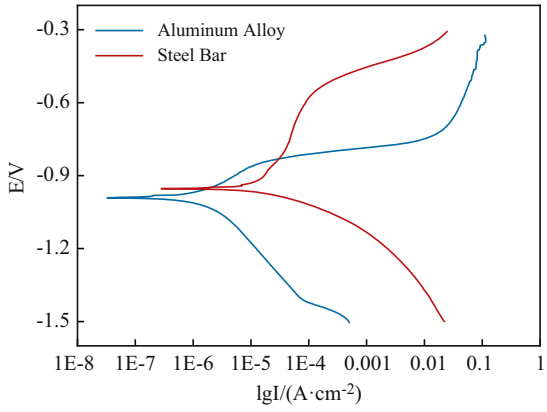

Figure 8: Polarization curves of aluminium alloy and steel bar in chloride solution.

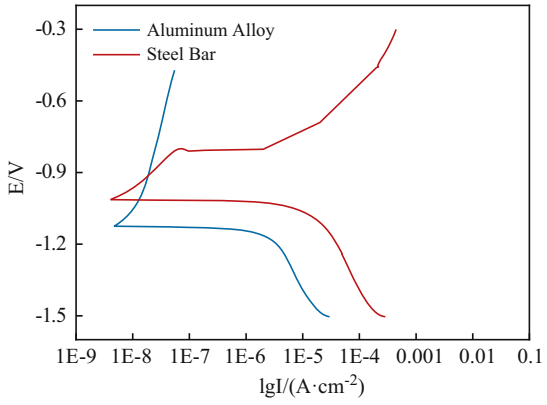

Figure 10: Polarization curves of steel bar and aluminium alloy in the simulated acid rain solution.

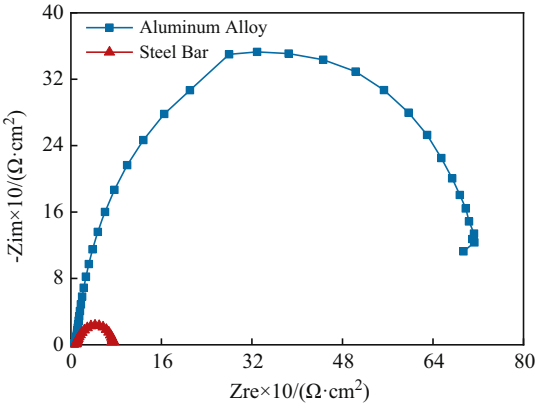

Figure 9: AC impedance spectroscopy of aluminium alloy and steel bar in the chloride solution.

solution. As can be seen from the figure, the impedance spectra of the aluminium alloy and steel bar in the corrosive medium after anodic oxidation show a single-capacitance arc with no "diffusive tail," indicating that the corrosion reaction is electrochemically controlled. The capacitance arc diameter of the aluminium alloy in the Nyquist diagram is much larger than that of the steel bar, which indicates that the impedance modulus of the aluminium alloy is higher and its corrosion resistance in the simulated acid rain solution is much better than that of steel bar. This is consistent with the conclusions obtained from the weight loss test.

3.3.3 Electrochemical characteristics in the saturated $Ca(OH)_2$ solution

3.3.3.1 Polarisation behaviour

Figure 12 shows the polarisation curves of the aluminium alloy and steel bar after soaking in a saturated $Ca(OH)_2$

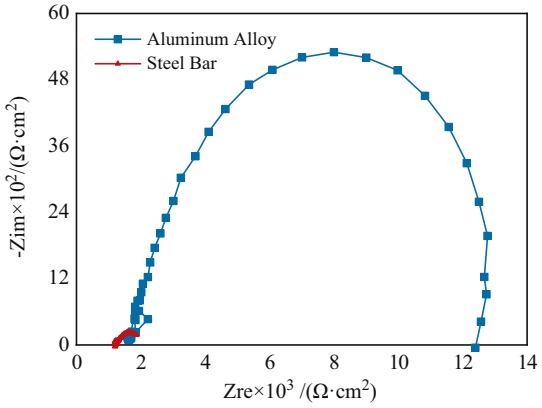

Figure 11: AC impedance spectroscopy of the aluminium alloy and steel bar in the simulated acid rain solution.

solution. The corrosion voltage of the aluminium alloy was −1.39 V, and its corrosion current was 0.22 μA·cm^{-2}. The corrosion voltage of the steel bar was −0.92 V, and its corrosion current was 0.005 μA·cm^{-2}. The self-corrosion potential of the aluminium alloy was significantly lower than that of the steel bar, while the self-corrosion current was much higher, which indicates that the corrosion rate of the aluminium alloy is faster than that of the steel bar.

In contrast, the steel bar is not easily corroded in a saturated $Ca(OH)_2$ solution. It can be seen from the polarization curve that when the anode potential increases to −0.92 V, the anode current density is insignificantly affected by the anode potential, which indicates that the anode begins to passivate. This is because the pH value of the saturated $Ca(OH)_2$ solution was as high as 12.5. In this strongly alkaline environment, a layer of a dense passive film forms on the surface of the steel bar, which hinders the electrochemical corrosion reaction.

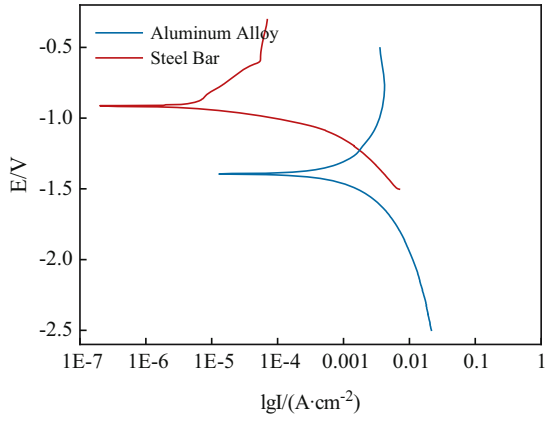

Figure 12: Polarization curves of the steel bar and aluminium alloy in the saturated $Ca(OH)_2$ solution.

3.3.3.2 AC impedance spectroscopy

The AC impedance spectra of the aluminium alloy and steel bar in the saturated $Ca(OH)_2$ solution are shown in Figure 13. It can be seen from the figure that the capacitive arc radius of the steel bar is much larger than that of the aluminium alloy, indicating that the corrosion resistance of the steel bar in the saturated $Ca(OH)_2$ solution is much better than that of the aluminium alloy, which is consistent with the conclusion of the above analysis.

3.4 Surface analysis of the 6061-T6 aluminium alloy

To further analyse the corrosion mechanism of the aluminium alloy in different solutions, the surface morphology of the corroded aluminium alloy was observed by scanning electron microscopy, and the composition of the corrosion products was determined.

3.4.1 Surface characteristics of the 6061-T6 aluminium alloy after corrosion by the chloride solution

3.4.1.1 Surface morphology

Figure 14 shows the surface morphology of the aluminium alloy after chloride corrosion. Pitting corrosion on the surface of the aluminium alloy is clear in the figure. The corrosion pits are irregularly round, and the thin corrosion products are in block or flocculent distribution. The formation of corrosion pits is due to the soluble chlorine complex when oxygen adsorption points on the

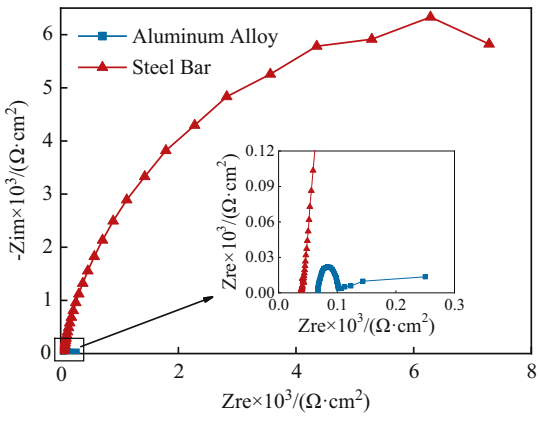

Figure 13: AC impedance spectroscopy of aluminium alloy and steel bar in the saturated $Ca(OH)_2$ solution.

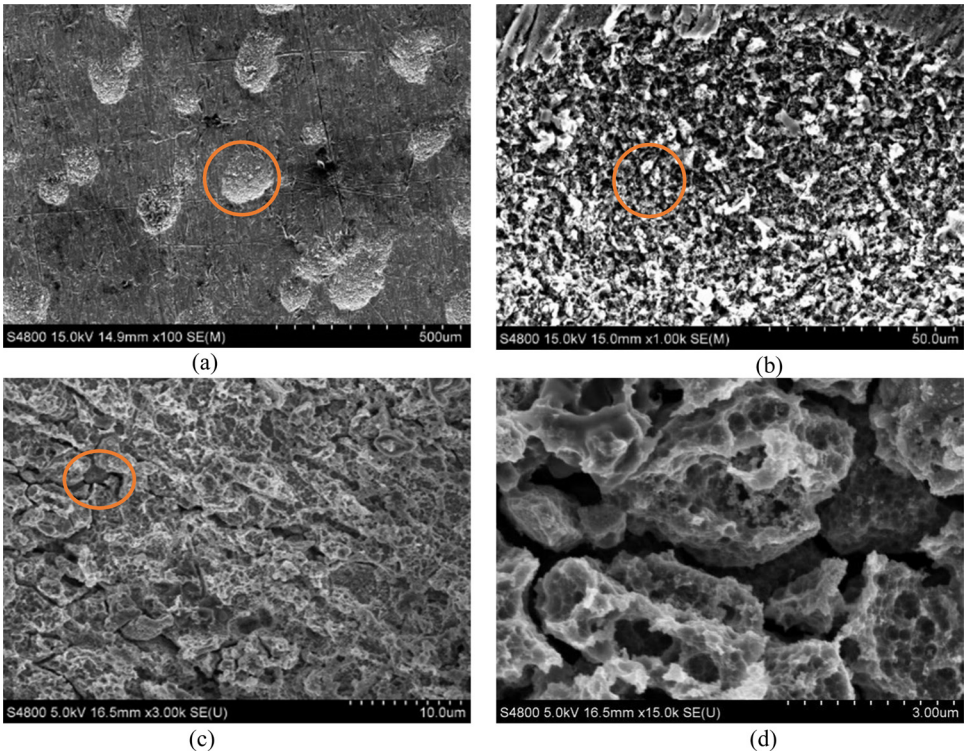

Figure 14: SEM micrograph of aluminium alloy corroded by chloride: (a) 29.8×, (b) 300×, (c) 1,650×, and (d) 5,500×.

surface of the aluminium alloy are replaced by chloride ions, resulting in the destruction of the passive film [38]. With the development of corrosion, the chlorine complex around the pitting corrosion also increased, and the area and depth of pits gradually increased.

3.4.1.2 Corrosion products

Figure 15 shows the EDS results of the corrosion products of the 6061-T6 aluminium alloy, and the elemental composition and atomic percentage of the corrosion zone are given in Table 7.

It can be seen from the EDS spectrum that the corrosion products mainly include Al, O, and other metal elements. This indicates that the corrosion products are mainly aluminium oxide, which is consistent with the previous research conclusion that the corrosion products are mainly Al_2O_3 and $Al(OH)_3$. Cl and Na were not detected, possibly because soluble ions were washed away during the cleaning process. Combined with the above electrochemical studies, it can be seen that in the initial stage of chlorine solution corrosion,

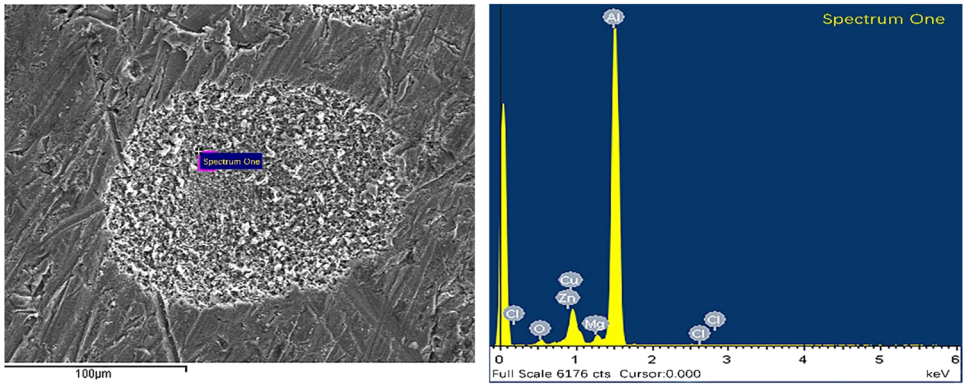

Figure 15: EDS analysis of chloride corrosion area of the aluminium alloy.

Table 7: Element analyses of corrosion products of the aluminium alloy (%)

Element	O	Mg	Al	Cl	Cu	Zn
Weight percentage	3.52	1.26	73.99	−0.12	15.29	6.05
Atomic percentage	6.57	1.55	82	−0.1	7.2	2.77

the surface of the aluminium alloy is oxidised and an $Al_2O_3{\cdot}H_2O$ oxide film is formed [39], as follows:

$$Al + H_2O \rightarrow AlOH + H^+ + e^-,$$

$$AlOH + H_2O \rightarrow Al(OH)_2 + H^+ + e^-,$$

$$Al(OH)_2 \rightarrow AlOOH + H^+ + e^-,$$

$$2AlOOH \rightarrow Al_2O_3 \cdot H_2O.$$

When $6 \le pH \le 9$, the corrosion product Al_2O_3 attaches to the surface of the aluminium alloy and forms a smooth and tight film layer. It seals the original corrosion crack and prevents the invasion of corrosion ions. The corrosion rate in the dissolution process is reduced, which causes the aluminium alloy to have good corrosion resistance. When the solution contains Cl^-, Cl^- is preferentially adsorbed on the active position (such as the defect location of the oxide film) on the surface of the aluminium alloy, reacts with the oxide film (such as the grain boundary), and forms $Al(OH)_xCl_{3-x}$ ($x \le 3$) until the aluminium surface film dissolves [40]:

$$Al(OH)_3 + Cl^- \rightarrow Al(OH)_2Cl + OH^-,$$

$$Al(OH)_2Cl + Cl^- \rightarrow Al(OH)Cl_2 + OH^-,$$

$$Al(OH)Cl_2 + Cl^- \rightarrow AlCl_3 + OH^-.$$

$Al(OH)_3$ on the surface of the aluminium alloy reacts with Cl^- to form $AlCl_3$, resulting in the dissolution of the aluminium element into the aqueous solution in the form of ions. The surface film of the aluminium alloy is destroyed, and the corrosion resistance is reduced. With an increase in corrosion time, the aluminium alloy potential increases and pitting corrosion occurs, forming a gully shape of corrosion products on the aluminium alloy surface.

3.4.2 Surface characteristics of the 6061-T6 aluminium alloy after corrosion by simulated acid rain

3.4.2.1 Surface morphology

Figure 16 shows the surface topography of the aluminium alloy after simulated acid rain corrosion at different magnifications. As seen from the figure, after 192 h of

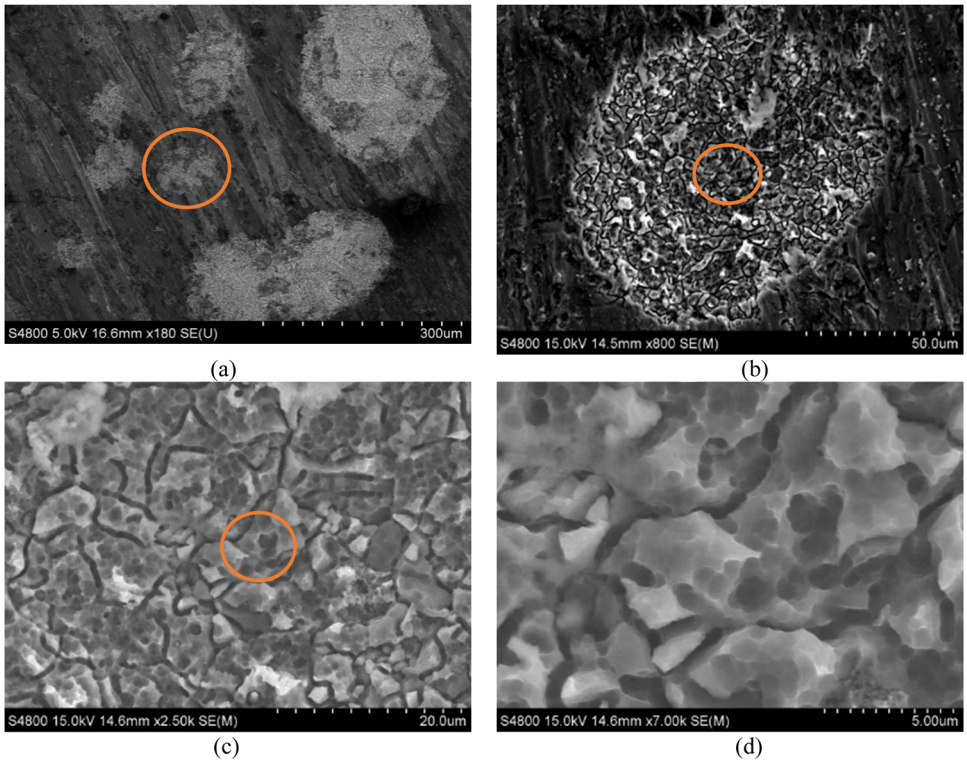

Figure 16: SEM micrograph of aluminium alloy corroded by simulated acid rain: (a) 55.3×, (b) 290×, (c) 730×, and (d) 2,920×.

corrosion by the acid rain solution, many corrosion products accumulated on the surface of the aluminium alloy. However, compared with corrosion by the chlorine solution, the simulated acid rain corroded mainly the metal surface, and the corrosion area was flaky, with a large area and small depth. The corrosion products in the pits were cracked with irregular shapes and continuously expanded. Because of the destruction of the passive film on the sample surface, the corrosive medium can easily invade the surface of the matrix, forming a large corrosion area.

3.4.2.2 Corrosion products

The surface energy spectrum analysis of the aluminium alloy soaked in the simulated acid rain solution for 192 h is presented in Figure 17, and the composition of the corrosion zone in an acidic environment is given in Table 8. Compared with the composition of the aluminium alloy before corrosion, the contents of S, Zn, and Cu on the surface of the aluminium alloy after acid rain corrosion increased. In the simulated acid rain solution with a low pH value, the dissolution rate of the surface film and aluminium matrix was faster, resulting in the enrichment of more Zn and Cu alloy elements. These alloying elements not only accelerate the dissolution of the matrix aluminium and enrich more alloying elements on the surface but also affect the corrosion potential of the aluminium alloy. Because the electrode potential of Zn and Cu is significantly higher than that of Al, and the corrosion potential of aluminium alloy reflects the mixed potential of the whole surface, the enrichment of Zn and Cu alloy elements on the surface may increase the corrosion potential of the aluminium alloy. Therefore, in the acid rain solution, with an increase in the precipitation rate and amount of alloy elements with a higher electrode potential than Al, the corrosion potential of the aluminium alloy increases.

Table 8: Element analyses of corrosion products of aluminium alloy 6061 (%)

Element	C	O	Mg	Al	S	Cu	Zn
Weight percentage	6.85	14.56	1.1	58.82	0.3	12.61	5.76
Atomic percentage	14.25	22.74	1.13	54.48	0.23	4.96	2.2

According to the localised corrosion principle of aluminium alloys proposed by Foley [41] and the above results, the corrosion of aluminium alloys in simulated acid rain solutions may involve the following processes: the competitive adsorption of ions in acid rain, such as Cl^-, SO_4^{2-}, NO^{3-}, OH^-, and H^+, and dissolved oxygen on the surface of the aluminium oxidation film. The adsorption occurred mainly at the defects of the oxide film, forming local corrosion pits, thinning the oxidation film, reducing the surface adsorption of ions and electrons through the resistance of the oxide film, and accelerating the reaction of active anions on the corrosion of the aluminium alloy matrix [42]. The highly active aluminium matrix dissolves and releases electrons to produce aluminium ions, which form intermediates with adsorbents and then desorb into the solution. The above process can be described as follows.

The anodic aluminium is dissolved:

$$Al \rightarrow Al^{3+} + 3e^-,$$

$$Al^{3+} + mX^{n-} \rightarrow Al^{3+}(X^{n-})_m.$$

The cathodic reaction is a reduction reaction of O_2 and H^+ ions:

$$O_2 + 4H^+ + 4e^- \rightarrow 2H_2O,$$

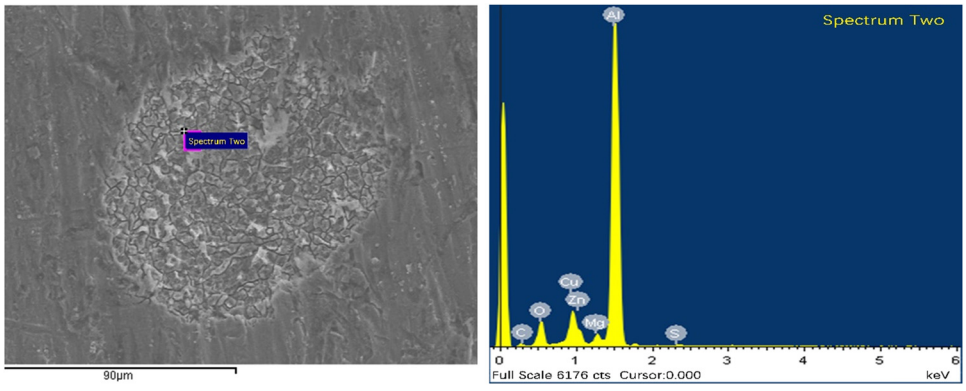

Figure 17: EDS analysis of simulated acid rain solution corrosion area of the aluminium alloy.

$$2H^+ + 2e^- \rightarrow H_2.$$

In the simulated acid rain solution with a pH value of 4.8, the surface oxide film dissolves slowly, and the anions in the solution adsorb at the surface defect site, which is either incorporated into the oxide film, or forms intermediate or stable corrosion products with Al^{3+}, thus hindering the further dissolution of the matrix.

3.4.3 Surface characteristics of the 6061-T6 aluminium alloy after corrosion by the saturated $Ca(OH)_2$ solution

3.4.3.1 Surface morphology

Figure 18 shows the surface morphology of the aluminium alloy corroded by the saturated $Ca(OH)_2$ solution. As can be seen from the figure, compared with the corrosion by chloride and simulated acid rain solutions with corrosion products only covering the shallow surface of the aluminium alloy, the scattered pits corroded by saturated $Ca(OH)_2$ have a relatively small corrosion area and large depth. The corrosion pits were filled with crystalline products, and some corrosion products fell off during the cleaning process. The severe corrosion of the 6061-T6 aluminium alloy in the saturated $Ca(OH)_2$ solution indicates that the alloy is not suitable for alkaline environments. In addition, as shown in Figure 17d, a large number of cracks and crystal particles appeared near the corrosion pit. During the test, the energy generated by the corrosion reaction of the alkaline solution caused the surface grains of the aluminium alloy to produce internal stress. When the residual stress is not completely eliminated, the nitric acid solution used for cleaning leads to uneven stress distribution, resulting in cracks on the surface layer and the formation of a denudation layer. The small white particles are crystals of corrosion products that are not completely removed.

3.4.3.2 Corrosion products

The composition and proportion of elements of the corrosion products in the corrosion area under an alkaline environment are presented in Figure 19 and Table 9, respectively.

Compared with the composition of aluminium alloy before corrosion, the contents of C, S, P, and alloy elements such as Fe, Zn, and Cu on the surface of the aluminium alloy increase after 192 h of saturated $Ca(OH)_2$ solution corrosion. Similar to corrosion by the acid rain solution, the hydroxide or oxide film on the aluminium surface will dissolve in an alkaline solution [42], resulting

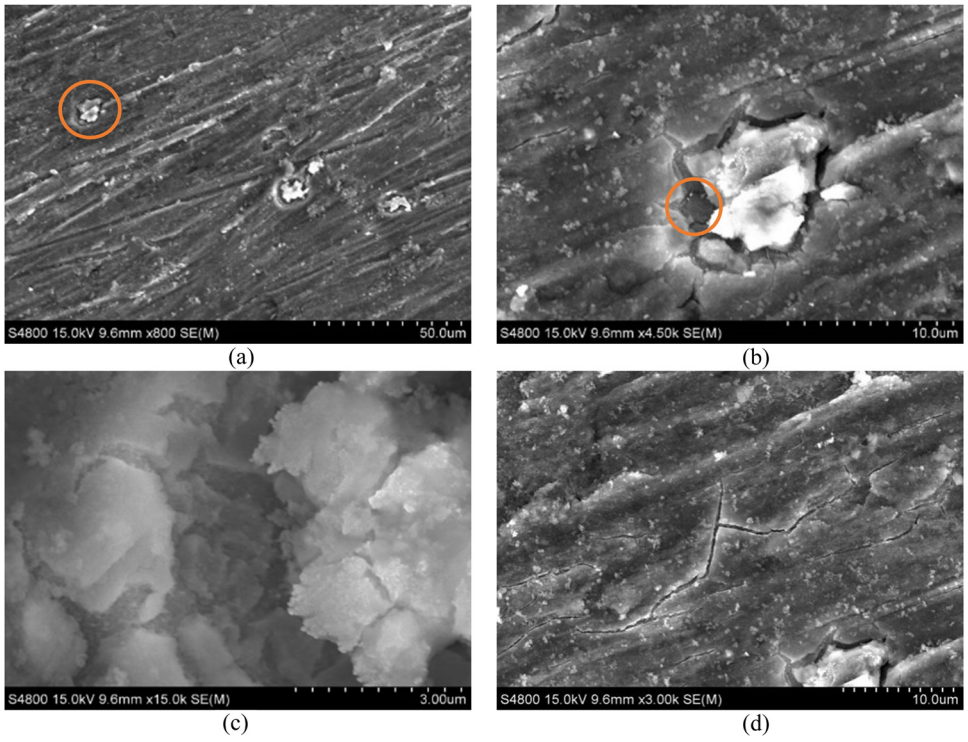

Figure 18: SEM micrograph of aluminium alloy corroded by saturated $Ca(OH)_2$ solution: (a) 192×, (b) 960×, (c) 3,200×, and (d) 960×.

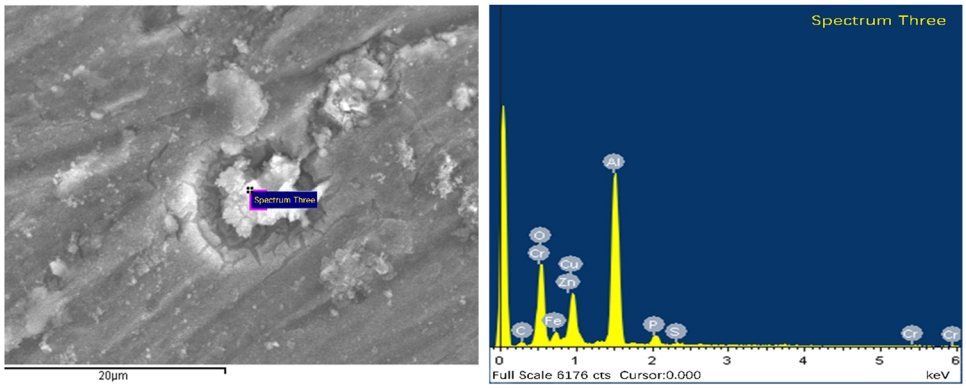

Figure 19: EDS analysis of the aluminium alloy under the corroded of the saturated $Ca(OH)_2$ solution.

Table 9: Element analyses of corrosion products of aluminium alloy 6061 after corrosion by saturated $Ca(OH)_2$ solution (%)

Element	C	O	Al	P	S	Cr	Fe	Cu	Zn
Weight percentage	6.56	28.83	28.06	2.16	0.39	0.56	7.42	22.22	3.79
Atomic percentage	13.58	44.81	25.86	1.73	0.30	0.27	3.30	8.70	1.44

in the enrichment of alloy elements such as Zn and Cu. This corrosion is often accompanied by hydrogen evolution [43]. The hydrogen evolution reaction occurs between the aluminium alloy matrix and the corrosion product adsorption layer, which has a considerable destructive effect on the corrosion product barrier layer. The reaction is as follows:

The anodic reaction is

$$Al + 4OH^- \rightarrow Al(OH)_4^- + 3e^-.$$

The cathodic reaction is

$$2H_2O + 2e^- \rightarrow 2OH^- + H_2.$$

As the corrosion reaction occurs on the aluminium alloy surface [44], the porous structure of the aluminium oxide film loses its protective effect in the dissolution and hydrogen evolution reaction [45,46]. The interaction between the film and the alloy matrix is enhanced, which leads to an increase in the film-induced stress and the initiation of cracks on the surface of the aluminium alloy. This is consistent with the surface morphology of the aluminium alloy mentioned previously.

The above research shows that the corrosion resistance of the 6061-T6 aluminium alloy is better than that of steel reinforcement when it is directly exposed to the natural environment, but its corrosion resistance is lower than that of steel reinforcement in concrete components. Therefore, considering the mechanical properties of 6061-T6 aluminium alloy reinforcement, it has good engineering value when used as external reinforcement.

4 Conclusions

In this study, the feasibility of using the 6061-T6 aluminium alloy in concrete structures was studied. Its corrosion behaviours in simulated coastal, atmospheric, and concrete internal environments were investigated. The results are as follows:

(1) The 6061-T6 aluminium alloy is classified as a corrosion-resistant material in chloride solution and simulated acid rain, with corrosion rates of 0.037 and 0.051 $mm \cdot a^{-1}$ and corrosion currents of 0.012 $\mu A \cdot cm^{-2}$ and 0.037 $\mu A \cdot cm^{-2}$, respectively. The steel bar is classified as an under-corrosion-resistant material in the above environments, with corrosion rates of 0.772 $mm \cdot a^{-1}$ and 1.319 $mm \cdot a^{-1}$ and corrosion currents of 0.078 $\mu A \cdot cm^{-2}$ and 0.082 $\mu A \cdot cm^{-2}$, respectively. Therefore, the corrosion resistance of the 6061-T6 aluminium alloy in coastal and atmospheric environments is much better than that of the steel bars.

(2) In the saturated $Ca(OH)_2$ solution, the 6061-T6 aluminium alloy, which is considered a non-corrosion-resistant material, has a corrosion rate of 16.166 $mm \cdot a^{-1}$ and a corrosion current of 0.22 $\mu A \cdot cm^{-2}$. Steel bar, which is protected by passivation films, is corrosion-

resistant. Therefore, the steel bar has better corrosion resistance than the 6061-T6 aluminium alloy in the internal concrete environment.

(3) In the early stage of corrosion, the surface of the aluminium alloy is mainly pitting corrosion. Acid rain corrosion occurs only on the surface of the aluminium alloy, the corrosion pits are flaky with a small depth, and the corrosion products crack intensely. In a chlorine environment, the corrosion pits of the aluminium alloy are deep, and the products, water-soluble $AlCl_3$, are distributed in the block or flocculent form. The saturated $Ca(OH)_2$ solution dissolves the hydroxide or oxide coating on the surface of the aluminium alloy, resulting in corrosion pitting of the alloy, and the corrosion pits are small and deep.

In summary, this study investigates the feasibility of applying 6061-T6 aluminium alloy reinforcement to concrete structures, and the corrosion law and corrosion products of 6061-T6 aluminium alloy under the possible service environment of concrete structures are also studied. The research results are helpful in expanding the usage of aluminium alloys in the construction industry, providing a reference for the application of aluminium alloy bars as external prestressed concrete bars and near-surface reinforcement bars and reducing the use of steel.

Funding information: This work was funded by the National Natural Science Foundation of China (Grant No. 51808438, 51868073) and the Youth Innovation Team Building Project of Shaanxi Provincial Department of Education (No. 21JP059).

Author contributions: Daming Luo: investigation, visualization, writing – original draft preparation; Fan Li: writing – review and editing, visualization; Guohua Xing: methodology, formal analysis, writing – review and editing.

Conflict of interest: The authors declare that there are no conflict of interest regarding the publication of this paper.

Data availability statement: The data used to support the findings of this study are available from the corresponding author upon request.

References

[1] Su, T., C. Wang, F. Cao, Z. Zou, and H. Yi. An overview of bond behavior of recycled coarse aggregate concrete with steel bar. *Reviews on Advanced Materials Science*, Vol. 60, No. 1, 2021, pp. 127–144.

[2] Sola, E., J. Ozbolt, G. Balabanic, and Z. M. Mir. Experimental and numerical study of accelerated corrosion of steel reinforcement in concrete: Transport of corrosion products. *Cement and Concrete Research*, Vol. 120, 2019, pp. 119–131.

[3] Hou, B., X. Li, X. Ma, C. Du, D. Zhang, M. Zheng, et al. The cost of corrosion in China. *Npj Materials Degradation*, Vol. 1, No. 1, 2017, pp. 1–10.

[4] Zhang, P., Y. Dai, W. Wang, J. Yang, L. Mo, W. Guo, et al. Effects of magnesia expansive agents on the self-healing performance of microcracks in strain-hardening cement-based composites (SHCC). *Materials Today Communications*, Vol. 25, 2020, id. 101421.

[5] Al Hasan, N. H. J., H. J. Alaradi, Z. A. K. Al Mansor, and A. H. J. Al Shadood. The dual effect of stem extract of Brahmi (Bacopamonnieri) and Henna as a green corrosion inhibitor for low carbon steel in 0.5 M NaOH solution. *Case Studies in Construction Materials*, Vol. 11, 2019, id. e300.

[6] Fang, H., X. Xu, W. Liu, Y. Qi, Y. Bai, B. Zhang, et al. Flexural behavior of composite concrete slabs reinforced by FRP grid facesheets. *Composites Part B*, Vol. 92, may, 2016, pp. 46–62.

[7] Liao, J., K. Y. Yang, , J. J. Zeng, W. M. Quach, Y. Y. Ye, and L. Zhang. Compressive behavior of FRP-confined ultra-high performance concrete (UHPC) in circular columns. *Engineering Structures*, Vol. 249, 2021, id. 113246.

[8] Dia, A., K. Robin, A. Riadh, and H. J. Du. Shear strengthening of RC beams using NSM CFRP bonded using cement-based adhesive. *Construction and Building Materials*, Vol. 301, 2021, id. 124365.

[9] Zhou, Y., M. Guo, L. Sui, F. Xing, B. Hu, Z. Huang, et al. Shear strength components of adjustable hybrid bonded CFRP shear-strengthened RC beams. *Composites Part B*, Vol. 163, 2019, pp. 36–51.

[10] Jeong, Y., W. S. Kim, V. Gribniak, and D. Hui. Fatigue behavior of concrete beams prestressed with partially bonded CFRP bars subjected to cyclic loads. *Materials*, Vol. 12, No. 20, 2019, id. 3352.

[11] Rakgate, S. M. and M. Dundu. Strength and ductility of simple supported R/C beams retrofitted with steel plates of different width-to-thickness ratios. *Engineering Structures*, Vol. 157, 2018, pp. 192–202.

[12] Zheng, X. H., B. L. Wan, P. Y. Huang, and J. L. Huang. Experimental study of hybrid strengthening technique using carbon fiber laminates and steel plates for reinforced concrete slabs. *Construction and Building Materials*, Vol. 210, 2019, pp. 324–337.

[13] Yang, L. J., Z. H. Deng, P. Liang, and H. F. Yang. Interfacial shear stress of reinforce concrete beam strengthened with aluminum alloy plate. *Journal of Civil and Environmental Engineering*, Vol. 42, No. 04, 2020, pp. 113–123.

[14] Abdalla, J. A., A. S. Abu-Obeidah, R. A. Hawileh, and H. A. Rasheed. Shear strengthening of reinforced concrete beams using externally-bonded aluminum alloy plates: An experimental study. *Construction and Building Materials*, Vol. 128, No. 15, 2016, pp. 24–37.

[15] Rajan, R., P. Kah, B. Mvola, and J. Martikainen. Trends in aluminium alloy development and their joining methods. *Reviews on Advanced Materials Science*, Vol. 44, No. 4, 2016, pp. 383–397.

[16] Reddy, B., S. R. Maity, and K. M. Pandey. Characterization of spray formed Al-alloys — A Review. *Reviews on Advanced Materials Science*, Vol. 58, No. 1, 2019, pp. 147–158.

[17] Kissell, J. R., R. L. Ferry. *Aluminum structures: a guide to their specifications and design*, John Wiley & Sons, New York, 2002.
[18] Zhang, Y., B. Y. Du, Y. Q. Wang, Z. X. Wang, and Y. W. Ouyang. Study of flexural–torsional buckling behaviour of 6061-T6 aluminium alloy unequal-leg angle columns. *Thin-Walled Structures*, Vol. 164, 2021, id. 107821.
[19] Montoya Z, R. D., E. L. Vera, Y. T. Pineda, and M. L. Cedeño. Effect of the layer of anodized 7075-T6 aluminium corrosion properties. *Journal of Physics: Conference Series*, Vol. 786, No. 1, 2017, id. 12032.
[20] Kharitonov, D. S., C. Örnek, P. M. Claesson, J. Sommertune, I. M. Zharskii, I. I. Kurilo, et al. Corrosion inhibition of aluminum alloy AA6063-T5 by vanadates: microstructure characterization and corrosion analysis. *Journal of the Electrochemical Society*, Vol. 165, No. 3, 2018, pp. C116–C126.
[21] Hosseini, S. A., A. Abdollah-zadeh, H. Naffakh-Moosavy, and A. Mehri. Elimination of hot cracking in the electron beam welding of AA2024-T351 by controlling the welding speed and heat input. *Journal of Manufacturing Processes*, Vol. 46, 2019, pp. 147–158.
[22] Ridvan, G., Y. Yakup, T. Emre, M. Faiz, and K. Ahmet. Improving wear resistance of 304 stainless steel reinforced AA7075 aluminum matrix composite by micro-arc oxidation. *Surface and Coatings Technology*, Vol. 368, 2019, pp. 15–24.
[23] Barros, P. D., J. L. Alves, M. C. Oliveira, and L. F. Menezes. Study on the effect of tension-compression asymmetry on the cylindrical cup forming of an AA2090-T3 alloy. *International Journal of Solids and Structures*, Vol. 151, 2017, pp. 135–144.
[24] Sun, Q., Q. Han, R. Xu, K. Zhao, and J. Li. Localized corrosion behaviour of AA7150 after ultrasonic shot peening: Corrosion depth vs. impact energy. *Corrosion Science*, Vol. 130, 2018, pp. 218–230.
[25] Kumar, R. S., S. S. Kumar, C. Rajendran, S. J. S. Chelladurai, and G. Balcha. Investigation on corrosion behaviour of LM25-SiCp composite using taguchi method. *Advances in Materials Science and Engineering*, Vol. 2022, 2022, id. 4341018.
[26] Krymsky, S. V., S. O. Sh, E. V. Avtokratova, M. M. Yu, and M. V. Markushev. Strength of cryorolled commercial heat hardenable aluminum alloy with multilevel nanostructure. *Reviews on Advanced Materials Science*, Vol. 31, No. 2, 2012, pp. 145–150.
[27] Bobruk, E. V., M. Y. Murashkin, V. U. Kazykhanov, and R. Z. Valiev. Aging behavior and properties of ultrafine-grained aluminum alloys of Al-Mg-Si system. *Reviews on Advanced Materials Science*, Vol. 31, No. 2, 2012, pp. 109–115.
[28] Zhu, S., M. Ohsaki, X. Guo, and Q. Zeng. Shape optimization for non-linear buckling load of aluminum alloy reticulated shells with gusset joints. *Thin-Walled structures*, Vol. 154, 2020, pp. 106830–106831.
[29] Tan, Y., Y. Zhang, Q. Zhang, and F. Fan. Static properties and stability of super-long span aluminum alloy mega-latticed structures. *Structures*, Vol. 33, No. 3, 2021, pp. 3173–3187.
[30] Kresse, G., M. Schmid, E. Napetschnig, M. Shishkin, L. Köhler, and P. Varga. Structure of the ultrathin aluminum oxide film on NiAl (110). *Science*, Vol. 308, No. 5727, 2005, pp. 1440–1442.
[31] Yu, X., G. Xing, and Z. Chang. Flexural behavior of reinforced concrete beams strengthened with near-surface mounted 7075 aluminum alloy bars. *Journal of Building Engineering*, Vol. 31, 2020, id. 101393.
[32] Ezuber, H., A. El-Houd, and F. El-Shawesh. A study on the corrosion behavior of aluminum alloys in seawater. *Materials & Design*, Vol. 29, No. 4, 2008, pp. 801–805.
[33] GB/T 19292.2-2018. Corrosion of metals and alloys-Corrosivity of atmospheres-Part 2, 2018.
[34] Angst, U. M. Correction to: Challenges and opportunities in corrosion of steel in concrete. *Materials and Structures*, Vol. 52, No. 1, 2019, id. 25.
[35] Liu, Y. J., Z. Y. Wang, and W. Ke. Corrosion behavior of 2024-T3 aluminum alloy in simulated marine atmospheric environment. *The Chinese Journal of Nonferrous Metals*, Vol. 23, No. 05, 2013, pp. 1208–1216.
[36] Hu, X., C. Shi, X. Liu, J. Zhang, and G. de Schutter. A review on microstructural characterization of cement-based materials by AC impedance spectroscopy. *Cement and Concrete Composites*, Vol. 100, 2019, pp. 1–14.
[37] Andrade, C. Propagation of reinforcement corrosion: principles, testing and modelling. *Materials and Structures*, Vol. 52, No. 1, 2019, pp. 1–26.
[38] El-Menshawy, K., A. A. El-Sayed, M. E. El-Bedawy, H. A. Ahmed, and S. M. El-Raghy. Effect of aging time at low aging temperatures on the corrosion of aluminum alloy 6061. *Corrosion Science*, Vol. 54, Jan., 2011, pp. 167–173.
[39] Abdel-Gawad, S. A., W. M. Osman, and A. M. Fekry. Characterization and Corrosion behavior of anodized Aluminum alloys for military industries applications in artificial seawater. *Surfaces and Interfaces*, Vol. 14, 2018, pp. 314–323.
[40] Li, S., H. G. Dong, L. Shi, P. Li, and F. Ye. Corrosion behavior and mechanical properties of Al-Zn-Mg aluminum alloy weld. *Corrosion Science*, Vol. 123, 2017, pp. 243–255.
[41] Foley, R. T., and T. H. Nguyen. The chemical nature of aluminum corrosion: V. Energy transfer in aluminum dissolution. *Journal of The Electrochemical Society*, Vol. 129, No. 3, 1982, pp. 464–467.
[42] Zhou, H., K. Li, C. Dong, and K. Xiao. Corrosion behaviors of aluminum alloy 2A12 under cyclic wet-dry immersion test in simulation solutions. *Equipment Environmental Engineering*, Vol. 4, No. 5, 2007, pp. 1–6.
[43] Araoyinbo, A. O., M. Abdullah, A. Rahmat, A. I. Azmi, and S. J. Tan. The effect of thermal treatment on the resistance of 7075 aluminum alloy in aggressive alkaline solution. *Journal of Science and Technology*, Vol. 10, No. 1, 2018, pp. 13–18.
[44] Song, H. M., X. D. Qin, L. Wang, and J. Y. Liu. The corrosion inhibition of sodium dodecyl benzene sulfonate on aluminum alloy in alkaline solution. *Journal of Inner Mongolia University of Science and Technology*, 2019, Vol. 38, No. 1, pp. 54–58.
[45] Park, I., S. Choi, and J. Kim. Aluminum anode for aluminum-air battery - Part II: Influence of in addition on the electrochemical characteristics of Al-Zn alloy in alkaline solution. *Journal of Power Sources*, Vol. 357, 2017, pp. 47–55.
[46] Aliramezani, R., K. Raeissi, M. Santamaria, and A. Hakimizad. Characterization and properties of PEO coatings on 7075 Al alloy grown in alkaline silicate electrolyte containing KMnO4 additive. *Surface & Coatings Technology*, Vol. 329, 2017, pp. 250–261.